Modeling the global micrometeor input function in the upper atmosphere observed by high power and large aperture radars

Diego Janches,[1] Craig J. Heinselman,[2] Jorge L. Chau,[3] Amal Chandran,[4] and Ronald Woodman[3]

Received 23 January 2006; revised 22 March 2006; accepted 31 March 2006; published 26 July 2006.

[1] We report initial results of an effort to model the diurnal and seasonal variability of the meteor rate detected by high power and large aperture (HPLA) radars. The model uses Monte Carlo simulation techniques and at present assumes that most of the detected particles originate from three radiant distributions with the most dominant concentrated around the Earth's apex. The other two sources are centered 80° in ecliptic longitude to each side of the apex and are commonly known as helion and antihelion. To reproduce the measurements, the apex source flux was set to provide ~70% of the total number of particles while the other ~30% is provided by the combined contribution of the two remaining sources. The results of the model are in excellent agreement with observed diurnal curves obtained at different seasons and locations using the 430 MHz Arecibo radar in Puerto Rico, the 50 MHz Jicamarca radar in Perú, and the 1.29 GHz Sondrestrom radar in Greenland. To obtain agreement with the observed diurnal and seasonal variability of the meteor rate, an empirical atmospheric filtering effect was introduced in the simulation which prevents meteors with low-elevation radiants ($\leq 20°$) from being detected by the radars at mesospheric altitudes. The filtering effect is probably produced by a combination of factors related to the interaction of the meteor with the air molecules such as electron production and/or the ablation at higher altitudes. On the basis of these results we calculate the micrometeor global, diurnal, and seasonal input in the upper atmosphere.

Citation: Janches, D., C. J. Heinselman, J. L. Chau, A. Chandran, and R. Woodman (2006), Modeling the global micrometeor input function in the upper atmosphere observed by high power and large aperture radars, *J. Geophys. Res.*, *111*, A07317, doi:10.1029/2006JA011628.

1. Introduction

[2] It is now widely accepted that extraterrestrial particles in the size range of 10^{-11} to 10^{-4} g are likely to be the major contributors of metals in the mesosphere/lower thermosphere (MLT) [*Williams and Murad*, 2002]. These particles come both from meteor showers and from the sporadic background complex. The latter provides a much greater input of material into the upper atmosphere than meteor showers [*Ceplecha et al.*, 1998; *Baggaley*, 2002]. It is also well established that this material gives rise to the upper atmospheric metallic and ion layers observed by radars and lidars. In addition, meteors are believed to be an important source for condensation nuclei (CN), the existence of which is a prerequisite for the formation of NLC particles in the polar mesopause region [*von Zahn et al.*, 2002]. In order to understand how this flux gives rise to these atmospheric phenomena, accurate knowledge of the global meteoric input function (MIF) is critical. This function accounts for the annual and diurnal variations of meteor rates, global distribution, directionality, and velocity and mass distributions. Estimates of most of these parameters are still under investigation.

[3] For example, the daily global amount of meteoric material is still not well defined and estimates vary by more than an order of magnitude, from ~7 to 250 tons of material a day over the whole planet [*Hughes*, 1978; *Wasson and Kyte*, 1987; *Love and Brownlee*, 1993; *Taylor*, 1995; *Mathews et al.*, 2001; *Cziczo et al.*, 2001]. In the past decade, high power and large-aperture (HPLA) radar meteor observations have also raised controversies regarding the geocentric velocity distribution of dust-sized particles. The very precise instantaneous micrometeor geocentric velocity distributions derived from these observations are faster than those derived from conventional lower frequency and low-

[1]Colorado Research Associates Division, NorthWest Research Associates Incorporated, Boulder, Colorado, USA.
[2]Stanford Research Institute International, Menlo Park, California, USA.
[3]Radio Observatorio de Jicamarca, Instituto Geofísico del Perú Lima, Perú.
[4]Department of Aerospace Engineering Sciences, University of Colorado, Boulder, Colorado, USA.

Copyright 2006 by the American Geophysical Union.
0148-0227/06/2006JA011628

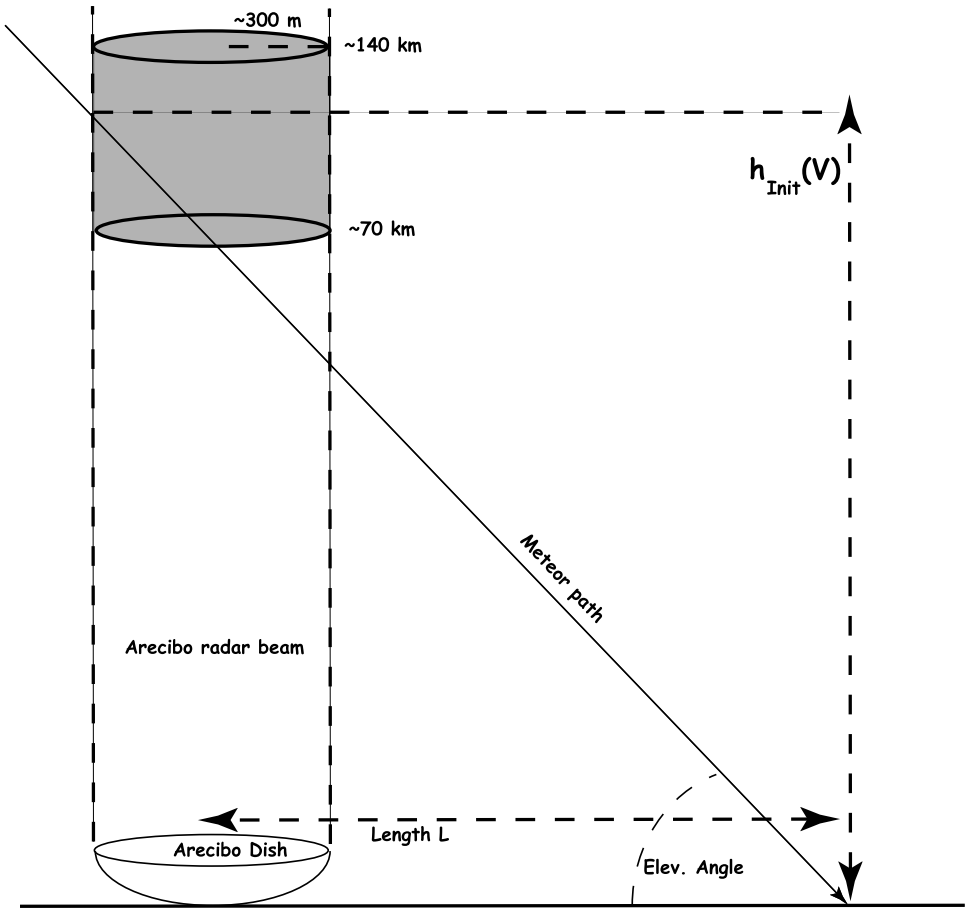

Figure 1. Diagram showing the assumptions made for the Monte Carlo simulation.

power meteor radars. [*Pellinen-Wannberg et al.*, 1998; *Close et al.*, 2000, 2002; *Sato et al.*, 2000; *Erickson et al.*, 2001; *Janches et al.*, 2000a, 2000b, 2001, 2002, 2003; *Chau and Woodman*, 2004; *Sulzer*, 2004; *Hunt et al.*, 2004]. The population of particles in the near-Earth interplanetary space is also under current analysis. Some recent work using different radio techniques [*Yrjölä and Jenniskens*, 1998; *Janches et al.*, 2001; *Chau and Woodman*, 2004; *Sulzer*, 2004; *Hunt et al.*, 2004] have failed to detect particles coming from some of the six accepted meteor sources describing the sporadic meteor complex [*Jones and Brown*, 1993; *Taylor*, 1997; *Taylor and Elford*, 1998]. Finally, since a better instrumental global coverage now exists we can begin to study the geographical variability of the meteoric influx. This is crucial because we cannot only study the average amount of material that is deposited over the whole atmosphere, but also when and where it is been deposited. For example, *Plane* [2004], in order to model the mesospheric Na layer, modulated the meteoric input with a seasonal and diurnal function resulting from the radio meteor survey reported by *Yrjölä and Jenniskens* [1998]. In order to understand globally how these metals are distributed in the MLT it is not only important to know this variability, but also how it is manifested geographically for a particular time of the day and year. Recently, *Janches et al.* [2004a] and *Singer et al.* [2004] reported meteor observation results from the Antarctic and the Arctic and showed that the activity is antisymmetric. In particular, when the seasonal maxima occurs at one hemisphere, the minima occurs at the opposite pole of the planet.

[4] We have started a theoretical, observational and modeling effort with the main goal of understanding how much, when and where micrometeor mass is deposited in the Earth's atmosphere. For this purpose we have developed a simple model that utilizes Monte Carlo simulation techniques with the goal to answer the following questions: Given a small volume placed in the MLT, what is the relative number of meteors that would intersect that volume and how does that number depend on geographical location and time? If this number can be effectively predicted, it would represent the first step toward an accurate estimation of the global MIF.

2. Micrometeor Input Function Model Description

[5] The model is constructed under the following basic assumptions (Figure 1).

[6] 1. We assume a flat Earth. This assumption is appropriate as long as the chosen volume is small as is the case for the HPLA radar illuminated volume in the MLT.

[7] 2. The radar observing volume is assumed to be a cylinder with the bottom placed at 70 km and the top at 140 km of altitude. The diameter of the cylindrical volume is first chosen to be 600 m, to simulate the case of Arecibo. This assumption is supported by the fact that the MLT can

be considered to be located within the Arecibo Observatory (AO) 430 MHz radar near field [*Breakall and Mathews*, 1982]. In this case the radar beam can be approximated as a cylindrical beam of the size of the ~300 m diameter dish. By doubling the size of the simulated observing volume we also include the first side lobes, a region where meteors are regularly detected at Arecibo [*Janches et al.*, 2004b].

[8] 3. We assume meteor populations with known radiant distributions. This assumption will be described in more detail in the next section.

[9] 4. We assume a micrometeor velocity distribution related to the chosen radiant distribution as explained in detail in the next section.

[10] 5. The mass function utilized for this model is based on a recent global influx curve estimated by *ReVelle* [2005], in which the Arecibo micrometeor measurements are compared with data obtained using infrasound [*ReVelle*, 2001] and satellite measurements [*Brown et al.*, 2002]. This new estimate shows that the number of meteors per mass bin is related to the initial meteor mass, in a log-log scale over twelve orders of magnitudes, by a straight line with a slope or mass index (α) approximately equals to one. To obtain this mass index we overlooked, for now, the saturation that is evident at small masses derived from early Arecibo observations [see *ReVelle*, 2005, Figure 7]. The reason for this is that we believe this saturation may result from a combination of atmospheric and/or astronomical physical factors which are not yet introduced in the model. In the first group the obvious factors are that small particles will not have enough energy to ablate and/or ionize upon their entry. If not enough electrons are produced and/or if the meteoroids are stopped in the MLT without significant heating and ablation, these particle will not be detected by the radar. There could be, however, additional astronomical effects related to the population characteristics of very small particles in the inner solar system. At present, the effect caused by the lack of inclusion of these factors in the model is that the total number of particles at a given time occurring within the modeled volume is much higher that the one measured. For now, however, we are more interested in the upper mass limit of the curve because, as is going to be discussed later, this will be directly related to the chosen diameter of the modeled detecting volume. We finally note that an $\alpha \sim 1$ has been proposed earlier for particles of the size range detected by HPLA radars [*Taylor*, 1995].

[11] 6. Another parameter we need to introduce in order to simulate the observed meteor rates is the altitude at which the meteor will be first detected by the radar, which will be a function of its velocity (h(V) in Figure 1). *Janches and ReVelle* [2005] showed that this altitude can be accurately calculated for the case of the Arecibo measurements using the meteor energy equation approximated for small particles (i.e., assuming thermal equilibrium across the interior of the particle). We apply the formulation presented in that work in this model. We note also that by using this approximation, the calculated initial altitude is independent of meteoroid mass.

[12] 7. Finally, *Janches and Chau* [2005] have also shown that having a radiant which elevation angle is above the local horizon is not a sufficient condition for a micrometeoroid to be detected by the radar. The authors suggested, from observational results of diurnal rates, that this effect may be caused by the ablation of meteoroids at higher altitudes. That is if the elevation is too low, the particles might ablate significantly before reaching the MLT. In this study, we introduce a simple empirical model in order to simulate this atmospheric interaction. This effect is represented by the definition of the threshold length L shown in Figure 1. If L is infinity, it implies that any meteoroid which radiant has an elevation above the local horizon will penetrate into the MLT and be detected by the radar. The other extreme value of L is 0 which implies that only meteoroids with vertical trajectories (elevation ~90°) will penetrate into the MLT and be detected by the radar.

3. Results

3.1. MIF at Arecibo (Latitude ~18°N, Longitude ~66°W)

3.1.1. Apex-Centered Radiant Distribution

[13] We first assume that the observed meteor population originates only from a radiant distribution centered around the Earth's apex. The distribution is modeled as a 2 dimensional gaussian with sigma equal to 32 and 16 degrees, in the ecliptic latitude and longitude respectively, in the heliocentric frame of reference. These parameters are taken from recent interferometric meteor head echo observations using the 50 MHz Jicamarca Radio Observatory (JRO) radar in Peru [*Chau and Woodman*, 2004], which showed that the velocity distribution of most of the meteors detected is clustered around the Earth's apex. The clustering of the measured meteor radiants are confined within the assumed sigmas in the solar-centered frame of reference and appears to be constant at all seasons. The JRO results are in agreement with previous results derived from both HPLA and traditional meteor radars. For example, *Jones and Brown* [1993], *Taylor* [1997], and *Taylor and Elford* [1998] described the sporadic meteor complex as formed by 6 sources. Two of these sources are the north and south apex (N/SA) which combined have the same characteristics as the JRO observed results. Furthermore, *Janches et al.* [2001] reported orbital properties of micrometeors observed by AO which showed agreement in the distribution of the orbital elements of the NA source. Finally, additional analysis of two different types of radar observations at Arecibo have confirmed the apex radiant as the main source of the Arecibo meteor detections [*Sulzer*, 2004; *Janches and Chau*, 2005].

[14] In accordance with the chosen radiant distribution, we assume the geocentric velocity distribution to be bimodal with a fast and dominant population centered at ~55 km/sec and a slower population centered at ~15 km/sec (Figure 2). The chosen distribution is taken from AO observations when the radar beam is pointed directly into the direction of the apex [*Janches et al.*, 2003; *Sulzer*, 2004; *Janches and Chau*, 2005] and hence assumed to be the total geocentric velocity distribution (i.e., not the radial component). This assumption is well supported by different investigations. For example, *Hunt et al.* [2004] derived the same velocity distribution from interferometric observations using the Advance Research Project Agency Long-Range Tracking and Instrumentation Radar (ALTAIR) system. This distribution is also in agreement with the velocity distribution of meteors from the NA and SA sources derived from conventional meteor

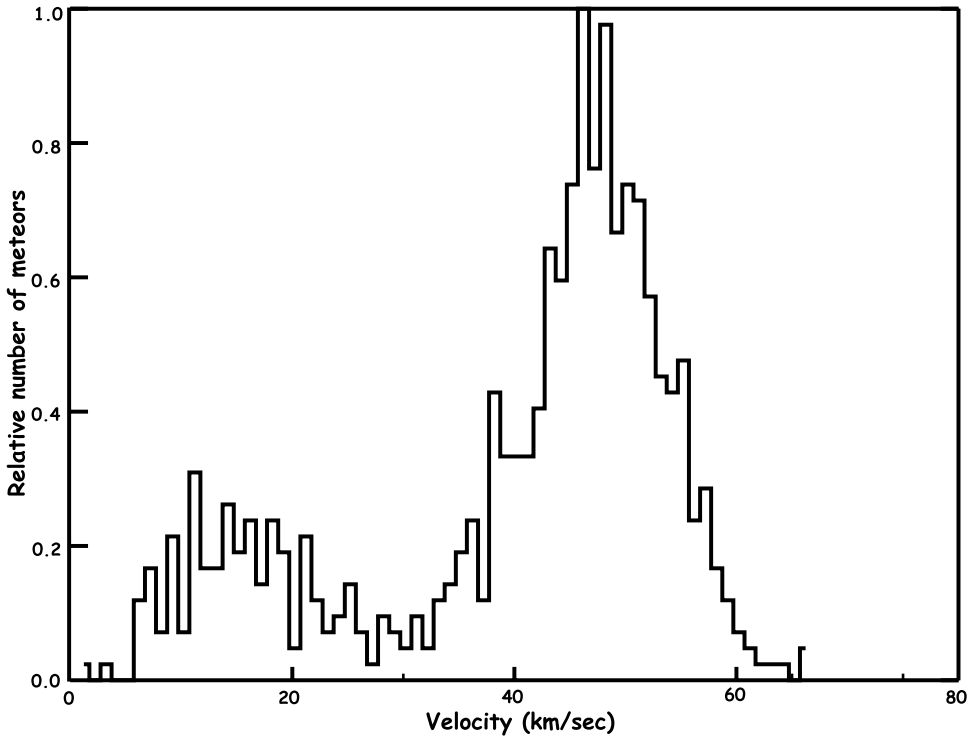

Figure 2. Assumed micrometeor velocity distribution. The chosen distribution is taken from AO observations when the radar beam is pointed directly into the direction of the apex [*Janches et al.*, 2003; *Sulzer*, 2004; *Janches and Chau*, 2005] and hence assumed to be the total geocentric velocity distribution (i.e., not the radial component).

radars [*Jones and Brown*, 1993; *Taylor*, 1997; *Taylor and Elford*, 1998]. It is important to note that HPLA and conventional meteor radars are two very different techniques which base their studies on the detection of two different scattering mechanisms [*Janches et al.*, 2003]. This implies that each technique introduces different biases to the observations and needs to be understood separately. A detailed discussion of this issue can be found in *Janches et al.* [2003] and *Janches and Chau* [2005]. It is evident now that HPLA radar are sensitive to a meteoroid population with significantly smaller sizes than the observed by traditional meteor radar techniques [*Janches and ReVelle*, 2005].

[15] Figure 3 shows a comparison between the predicted and observed meteor rates at Arecibo for 21 January 2002. For this comparison we assume that as long as the meteor radiant is above the local horizon particles originating from the chosen distribution will be detected by the radar ($L \sim \infty$). Most of the observations presented in this paper started in the early evening and ended at 08:00 AST of the following day. That is why the observed curve in Figure 3 ends abruptly at that local time. It is evident from this figure that the predicted flux does not match the observed one. The disagreement shown in Figure 3 indicates that a meteor radiant above the local horizon is not a sufficient condition for the observation of these particles as already shown by *Janches and Chau* [2005].

[16] We now explore the effects that different L values introduce to the model and we compare in Figure 4 again the predicted rates with the observed ones on 21 January 2002. For these comparisons we use three different L values (100, 200, and 400 km). We can observed in these panels that for a $L \sim 200$ km the agreement between data and model in the first half of the diurnal curve is excellent. After $\sim$05:30 AST, when the peak of the diurnal rate is reached, the observed rate seems to decrease more rapidly and earlier than the model predicts. In a previous work [*Janches and Chau*, 2005] we suggested the possibility that this difference could be produced by the stronger radar return from the background ionosphere that occurs after the Sun rises. In that case, meteors with low SNR could become more difficult to detect. The analysis of data at different seasons shows this is not the case.

[17] The panels in Figure 5 present the comparison between the model and the observed data for the rest of the months. The details of the AO observations can be found in *Janches et al.* [2003]. Each predicted curve is normalized to fit an average of the maxima of the corresponding measured curve. The normalization factor used is the same for each single months which indicates that the seasonal variability is also modeled as it is discussed later in this section. For the diurnal curve measured on 14 February 2002 (Figure 5a) we found that an $L \sim 200$ km is also needed to get agreement between observations and model. However, for the observations obtained after 25 March 2002 (Figures 5b–5k), agreement between model and data is found only when we increase the L value to 400 km instead of 200 km. This increment effectively decreases the radiant threshold from $\sim$26° to $\sim$15° in elevation. That is, particles with radiants below this threshold do not seem to be observed by the radar. In the next section we will

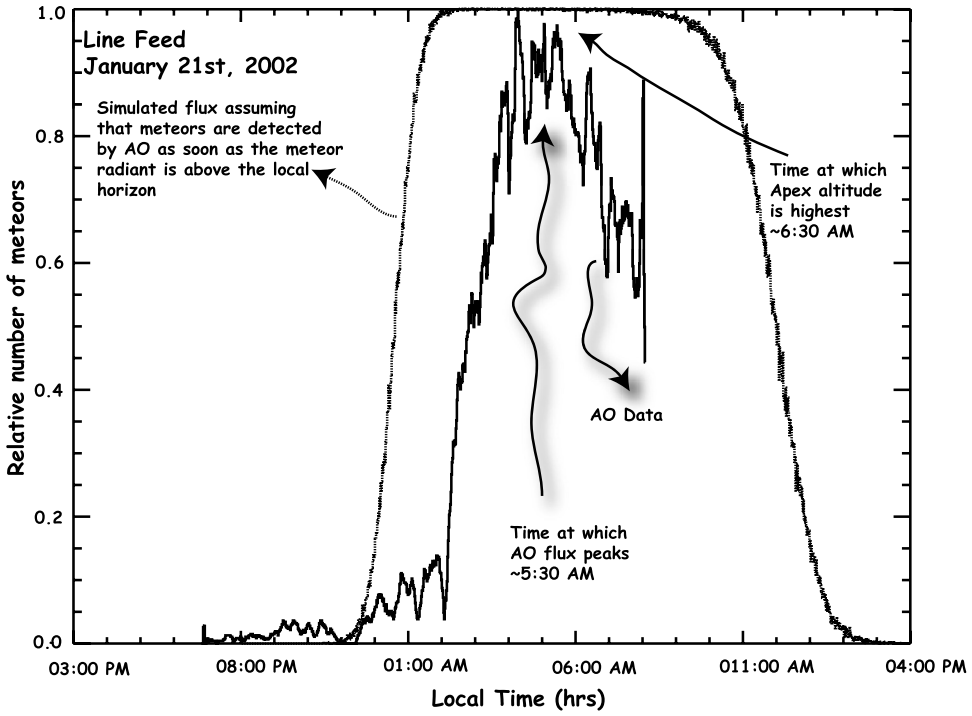

Figure 3. Comparison between the predicted and observed meteor rates at Arecibo for 21 January 2002 assuming that, as long as the meteor radiant is above the local horizon, then particles originating from the chosen distribution will be detected by the radar ($L \sim \infty$).

show that this difference is an artifact of an other source. A surprising feature that becomes evident also in the March and later observations is that the observed meteor rate appears to decrease earlier than the model predicts, reaching a local minimum around 06:30–07:00 local time, and rapidly increases to follow the predicted modeled curves. This effect is very well pronounced for the observations performed on 25 June 2002 and later months (Figures 5e–5k). In particular it can be observed from the observations for 21 September 2002 (Figure 5h) that the final daily decrease of the observed rate follows the predicted curve very well. Unfortunately, these are the only observations currently available that cover that time period. Another interesting feature that can be seen in Figures 5g and 5k (the only times we have observations from both side of this feature or dip) is that although the flux increases again, it appears to be to a lower peak than before the dip.

3.1.2. Contributions of the Helion and Antihelion Meteoroid Sources

[18] Aside from the January/February difference in the parameter L and the dip in the observed diurnal curves, it is evident that the predicted meteor rate resulting from these simple assumptions shows good agreement with the general diurnal trend of the observations. This suggests that, overall, an apex-centered distribution is sufficient to reproduce the general large-scale diurnal trend of the Arecibo measurements, but does not explain the small temporal-scale details. In order to investigate the origins of these observed features we introduce the contribution of two other known meteor radiant distributions known as the helion and antihelion sources [*Jones and Brown*, 1993; *Taylor*, 1997; *Taylor and Elford*, 1998]. They are also centered around the ecliptic plane $\sim 80^\circ$ to each side of the Earth's apex direction with sigma values in the ecliptic longitude and latitude approximately equal to half of the apex [*Jones and Brown*, 1993]. We assume that the overall contribution of these sources is a third of that from the apex one (a sixth for each secondary source). This factor results in the best agreement between data and model as shown in the panels in Figure 6 for every month of 2002 and for an assumed $L \sim 400$ km. It is evident from this figure that the additional contribution of these two sources reproduces fairly accurately the smaller-scale features of the observed rates. The dip in the rate is now predicted and surprisingly its characteristics are seasonally dependent. For example, there is no signs of a dip in the first five months of the year. Instead, during this time it can be seen that the peak of the distribution shift from ~05:00 LT in January to ~09:00 LT in May with a flatter top in March (spring equinox), at the middle of this period. In addition, although the January measured rates seem to be too large compared with the predictions, the behavior of the diurnal curve during this month is modeled well. As mentioned earlier, the peak of the flux at this time of the year is reached earlier in the morning, decreasing sharply after the rate maximizes. This effect is both measured and modeled (Figures 6a and 6b). Also, the measured rate increases in January and February still occurs later than the predicted model. Starting in June, the dip in the rates becomes evident and manifests seasonal variability during the later half of the year which is again both modeled and measured. During June, July, and August the second peak is larger than the first one, indicating that at Arecibo-like latitudes, the helion contribution during this part of the year is larger than the antihelion. During the autumn equinox, the distribution

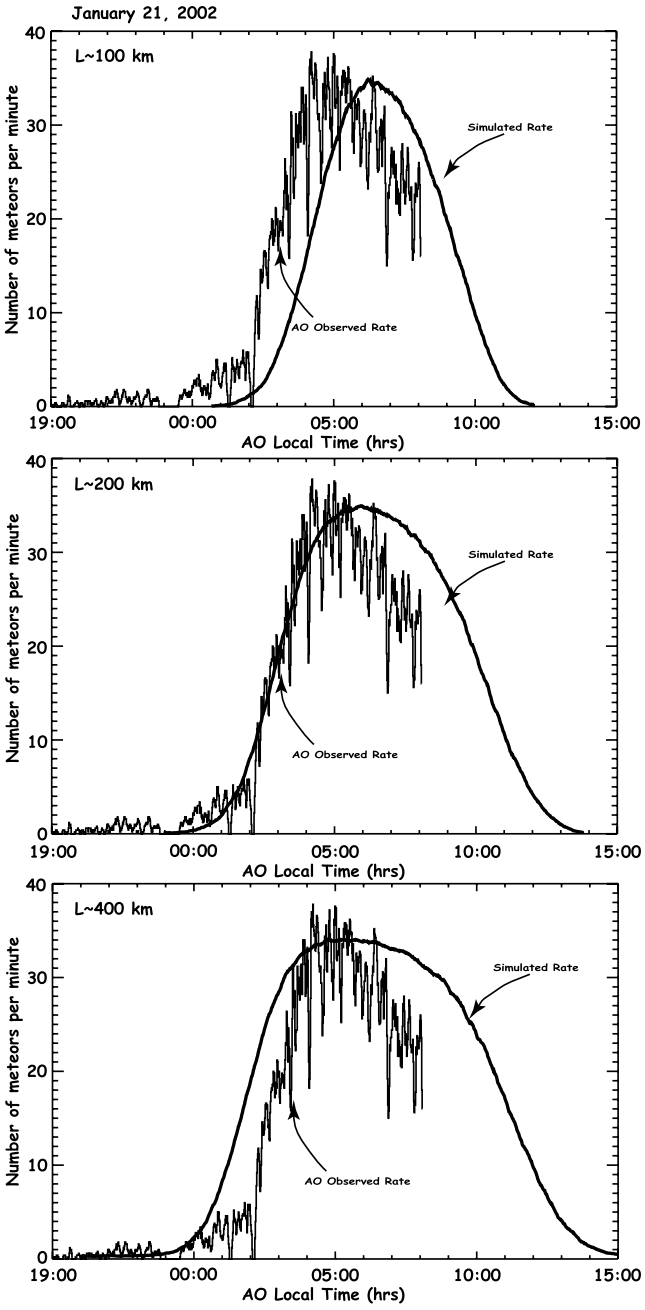

Figure 4. Comparison of predicted rates with the observed ones on 21 January 2002. For these comparisons we use three different L values (100, 200, and 400 km).

seems to be symmetric around ~06:00 LT, and after this time the first peak becomes increasingly more dominant, suggesting a stronger contribution from the antihelion source on the MLT at the Arecibo Observatory geographical location. Although our measurements do not cover the whole period of time to unequivocally verify that this behavior is observed, most of these features are nevertheless evident in the data. For example, in September, Figure 6i, we started our observation right at the time of the dip and the data follows very accurately the rate recovery and final daily decrease. In addition, in December, Figure 6l, our observations lasted until 10:00 LT, and we can observe that as predicted, the meteor rate after the dip is lower than the first peak. Figure 7 displays observations performed during 2004 and 2005 which covered period beyond 08:00 LT and again we can see that the predicted rates follow the observed rates generally well.

[19] The seasonal and diurnal variability on the small-scale features of the meteor rates suggest that for a given small volume in the MLT at the Arecibo latitude, the contribution of the different meteor radiant distributions to the meteoric mass flux varies throughout the year. Since particles from different radiant distribution, or orbital families, have different origins, cometary and/or asteroidal, they most likely also have different compositions. This would indicate that for a given latitude the composition of the material being deposited in the upper atmosphere could vary seasonally.

[20] There are still some discrepancies between observations and model. For example, the measured rates in January and June seem to be much larger when compared with other months and the predicted seasonal variation. Also, the observed diurnal curve on 15 March 2005 (Figure 7b) also show some variability which is not predicted after reaching the peak. Future observations will provide additional information as to whether these are real observational features.

[21] From the agreement found between prediction and observations at different seasons and even years, it is natural to assume that the model presented in this work will predict equally well the shape of the diurnal meteor rate observed above AO every other day during a given year. In Figure 8 we show the predicted meteor rate that should be detected in the small observed volume for the full year at Arecibo. As can be seen from this image, for a given small volume in the MLT region above Arecibo, the micrometeor rate will be minimum on 21 March when the highest elevation of the Earth's apex in the Arecibo local sky is lowest compared with other seasons [*Sulzer*, 2004; *Janches and Chau*, 2005]. Such a feature has been reported in the meteor observations at Arecibo and other radars [*Janches and Chau*, 2005; *Dyrud et al.*, 2005]. In the case of Arecibo, the observed rate in March decreases almost half of the rate measured in January or June (Figure 5). *Janches and Chau* [2005] also suggested that on 21 September the meteor rate observed at AO should be maximum because of the same geometrical effect. During this day the highest elevation of the apex is maximum for all seasons in the Arecibo sky. However, the geometrical and atmospheric filtering effects discussed here manifest in a somewhat different manner than previously suggested. The maximum micrometeor rate is reached early in June and it remains constant until late December/early January. The duration of the maximum rate, on the other hand, shows seasonal dependence lasting up to ~6 hrs during the autumn solstice. As mentioned earlier, the relative contribution of the other sources also manifest a seasonal variability. The later peak (contribution from helion source) appears in May and disappears in late November. The earlier peak on the other hand (contribution from the antihelion source) it is not evident until after the summer solstice and lasts until late February.

[22] The predicted seasonal variability on the meteor rates is also modeled very well as it is evident from the panels in Figure 6. First, the relation between the rates measured in March and those measured in the last 6 months seems to

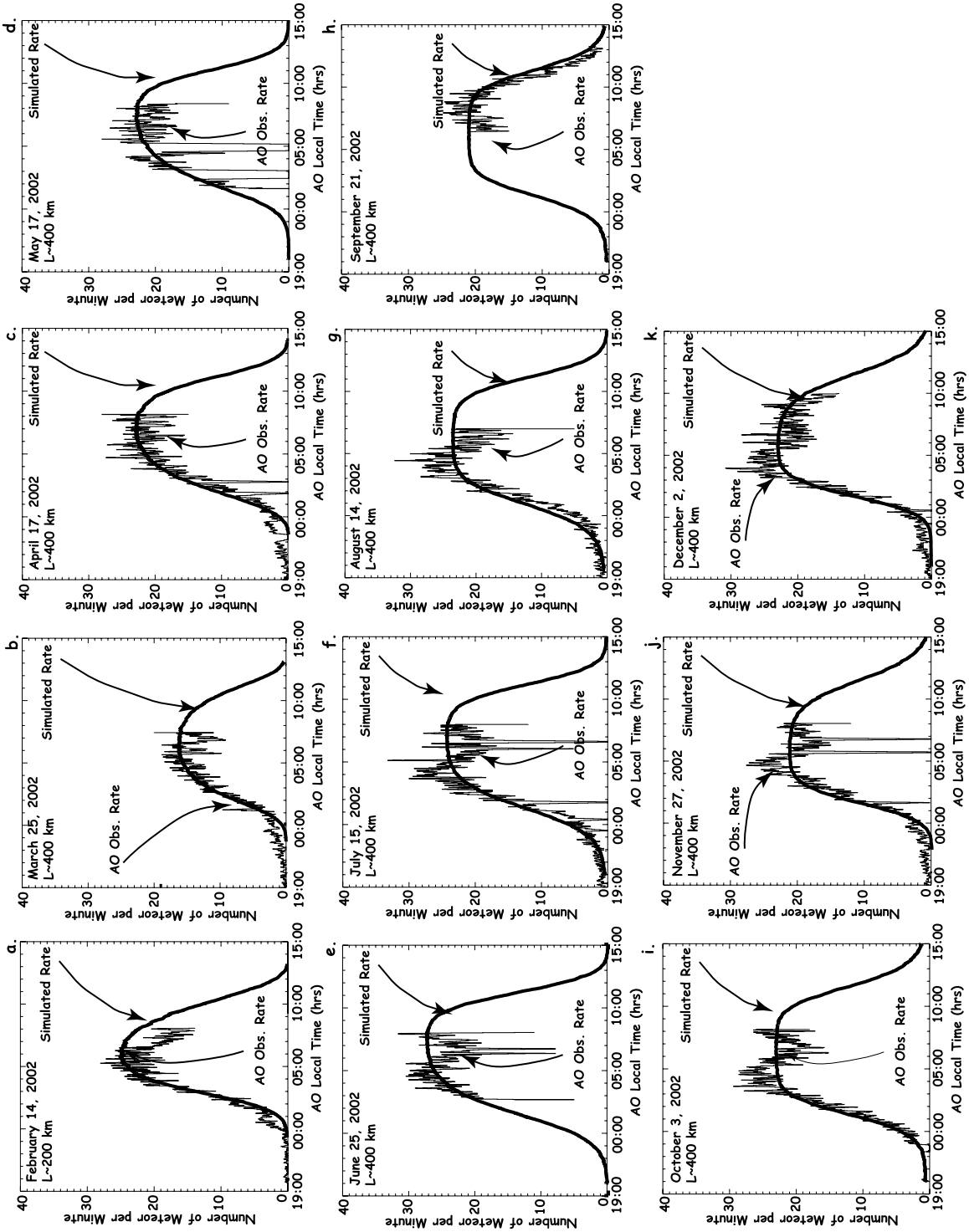

Figure 5. Comparison between the model and the observed data for the rest of the months. The details of the AO observations can be found in *Janches et al.* [2003]. Each predicted curve is normalized to fit an average of the maxima of the corresponding measured curve.

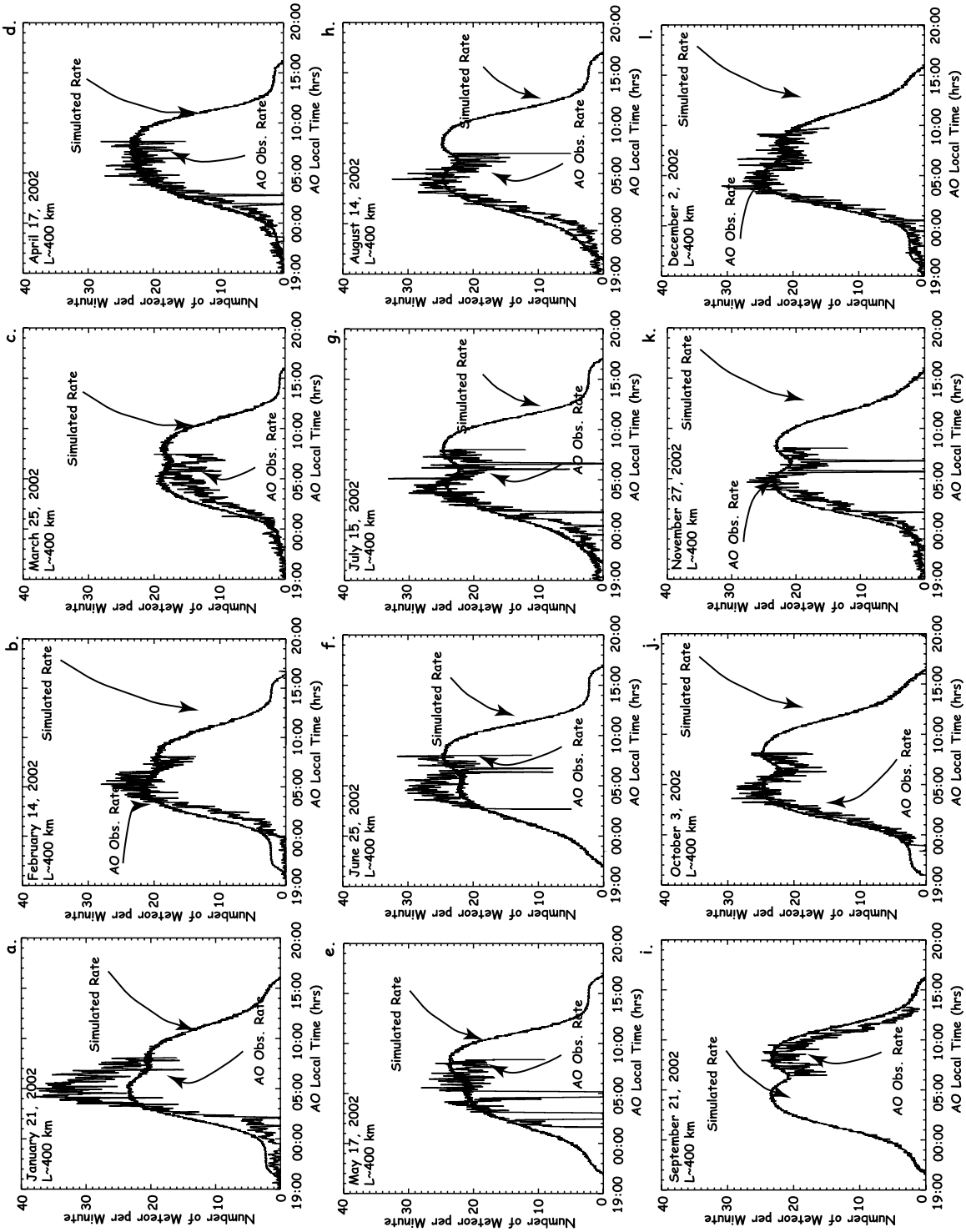

Figure 6. Comparison between the model and the 2002 observed data with the inclusion of the helion and antihelion sources.

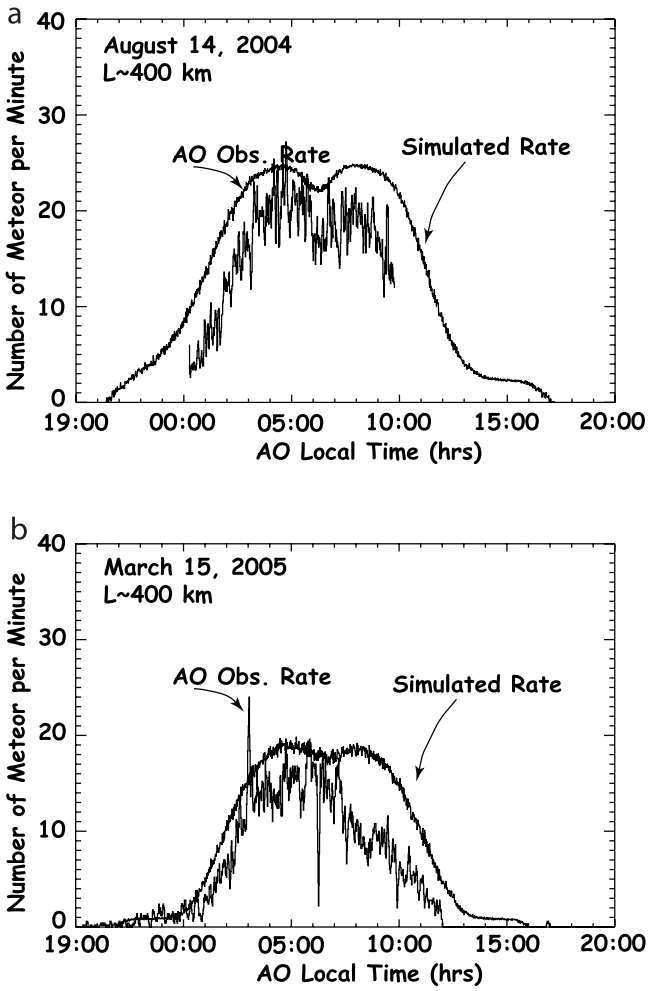

Figure 7. Same as Figure 6 but for observed data in August 2004 and March 2005.

follow the predicted curve. For example, calculating the ratio of the daily maximum to that of 21 September for the days in March for which observations are available results in ~0.72 and ~0.69 for the modeled and measured rates respectively. It can be noted also from Figure 6 that the maximum rates in the last 6 or 7 months of 2002 are fairly constant as predicted by the model. On the other hand, as we mentioned earlier the rates observed in January and June are particularly much higher than predicted. Also the decrease in the rates from January to March and the increase from March to May seem to be more pronounced than the modeled one. We are currently programming observations during the springtime, when most changes seem to occur, as well as the inclusion of more sophisticated ablation and electron production models into the simulation which will provide more information on this variability.

3.2. MIF at JRO (Latitude ~12°S, Longitude ~77°W)

[23] Since we find general agreement between the predicted and observed seasonal and diurnal behavior of the meteor rate at Arecibo, we can now attempt to simulate the diurnal and seasonal meteoric rate at other geographical locations. Obtaining full diurnal coverage of the meteor activity using the JRO system is challenging because of the presence of the ionospheric electrojet. When the jet is active, the return from the ionosphere is so strong that it is very difficult to separate meteor signals from the background. Although observations have been performed at very different times using this radar [*Chau and Woodman*, 2004; *Janches and Chau*, 2005], at present we obtained only one fairly complete diurnal curve presented in Figure 9. This curve was obtained by integrating three consecutive days of observations in November 2002. In Figure 9 we also show the predicted rates where the effects of the secondary sources in the small-scale variability is evident. The agreement between data and model shown in Figure 9 is once again excellent. An ongoing effort which utilizes sophisticated signal processing technique may be able to provide more often complete diurnal curves in the near future. Because of the agreement shown in Figure 9 we assume once again that the model will predict equally well the rate measured by JRO every other day of the year. Figure 10 shows the predicted meteor rate at JRO (~12°S, 77°W). showing a somewhat similar behavior to Arecibo but inverted in time. This makes sense since JRO is located in the Southern Hemisphere. The minimum rate is now predicted to occur on 21 September, the Southern Hemisphere spring equinox. Also note, that since JRO is closer to the Earth's equator than AO, the ratio of maximum daily rate between spring and autumn is lower than at AO.

3.3. MIF at Sondrestrom (Latitude ~67°N, Longitude ~51°W)

[24] We now simulate the flux at a high northern latitude (~67°N; ~51°W) which is the case for the 1.29 GHz Sondrestrom radar in Greenland and show the comparison of the model with actual observed rates at this location in Figure 11. For this comparison, the diameter of the modeled volume was increase to 1 km since the Sondrestrom radar beam is wider than the Arecibo one. The observations displayed here were obtained during late summer/spring and autumn months in three different years. Although the earlier observations were performed during the Leonids meteor shower period, it has been largely accepted now that HPLA radars do not seem to be effective at detecting showers and most, if not all, of the detections are due to sporadic activity [*Janches et al.*, 2001, 2002; *Chau and Woodman*, 2004; *Hunt et al.*, 2004]. The model results are once again fit to the measured maximum rate observed at Sondrestrom. First it is important to note the low rate of meteors shown in Figure 11. During the autumn months there is ~1 meteor per minute detected at the peak of the diurnal curve compared with ~25 in the Arecibo observations (Figures 5 and 6). Although the low meteor rate is predicted by the model it is likely that the higher radar frequency utilized in Sondrestrom also contributes to the low count. The frequency-dependent scattering mechanism of the head echo precludes detections at higher frequencies and reduces the head echo SNR, thereby making it more difficult for higher-frequency radars to detect head echoes [*Close et al.*, 2002]. More details on this issue are discussed at the end of this section. Nevertheless, during the autumn months when the detected meteor count is sufficiently high, once again the agreement in the diurnal variability between observations and predictions is excellent. It can also be argued that the October rate is somewhat higher than the

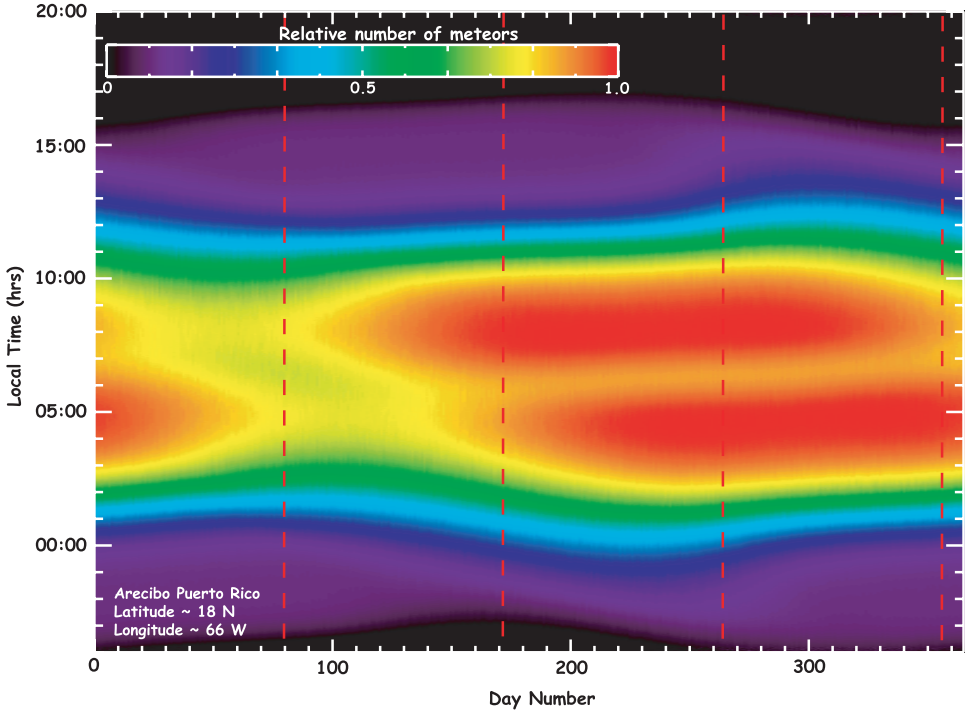

Figure 8. Predicted meteor rate that should be detected in the small observed volume for the full year at Arecibo-like latitudes.

one measured in November. During the late summer and spring months the observed count rates are very low but the agreement with the predicted diurnal trend is good. It is important to notice that the low count rate during springtime is also predicted by the model.

[25] We also calculated the influx for a full year at this location and the results are shown in Figure 12. As expected, the seasonal variability looks very different than that at lower latitudes. There is a large depletion on the micrometeor input in spring that extends for several months and a sharp increase toward the autumn equinox. Once this time of the year is reached the maxima last similar periods of time as at lower latitudes but the flux does not seem to drop to zero. This is related to the fact that at this latitude and during this time of the year, at least a small portion of the radiant distribution will always be above the elevation threshold set by L in this model. The ratio of spring to autumn is much larger than at lower latitudes, again because during the spring only a small portion of the radiant distribution will appear above the elevation threshold. The contribution of the secondary sources also do not manifest separately like at lower latitudes.

3.4. Global MIF

[26] Since our model shows great agreement with the seasonal and diurnal observations performed at Arecibo and suggests an equal type of agreement with observations at a high northern latitude, it is natural to assume that it can be used to predict the micrometeor rate over the whole range of latitudes from these sporadic particle populations. A set of predictions every 5° in latitude for the 15th of each month at a longitude of ~66°W is shown in the panels of Figure 13. In this picture a seasonal variation is observed which is largest at higher southern and northern latitudes. For example, in February the predicted meteor activity increases at southern latitudes greater than 50 degrees, reaching a maximum in March (Southern Hemisphere autumn) and a minimum in September (Southern Hemisphere spring). An equal behavior is shown in the Northern Hemisphere where the maximum is reached during the autumn months (September) and the minimum around spring (March). Also at these high latitudes, once the activity is high, the diurnal variability is lower. In particular, at or near the poles the model predicts practically no diurnal variability. *Janches et al.* [2004a] presented meteor radar observations using a system located at the South Pole. The authors showed that the observed rate is minimum in spring and maximum in the summer months (December–January). They also showed

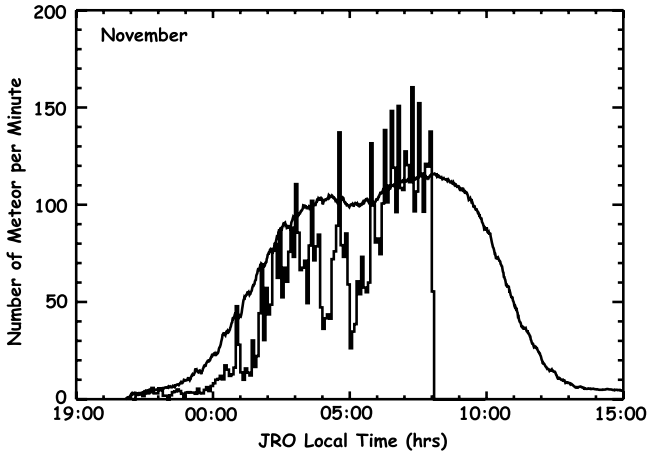

Figure 9. Comparison between prediction and observed rates at JRO for November 2002.

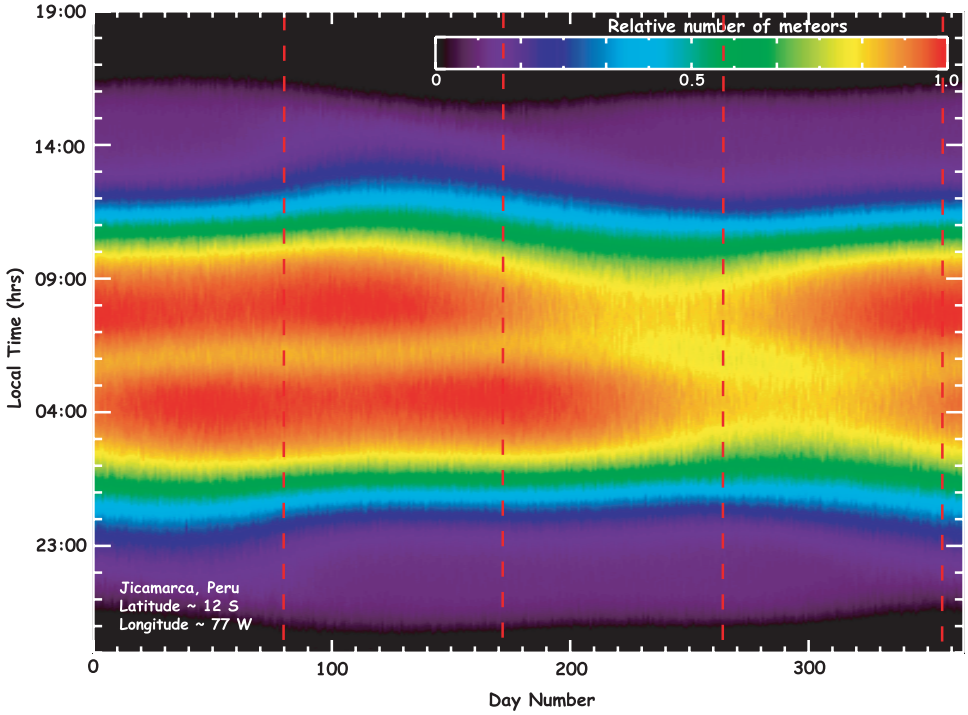

Figure 10. Predicted yearly meteor rate at JRO (∼12°S, 77°W).

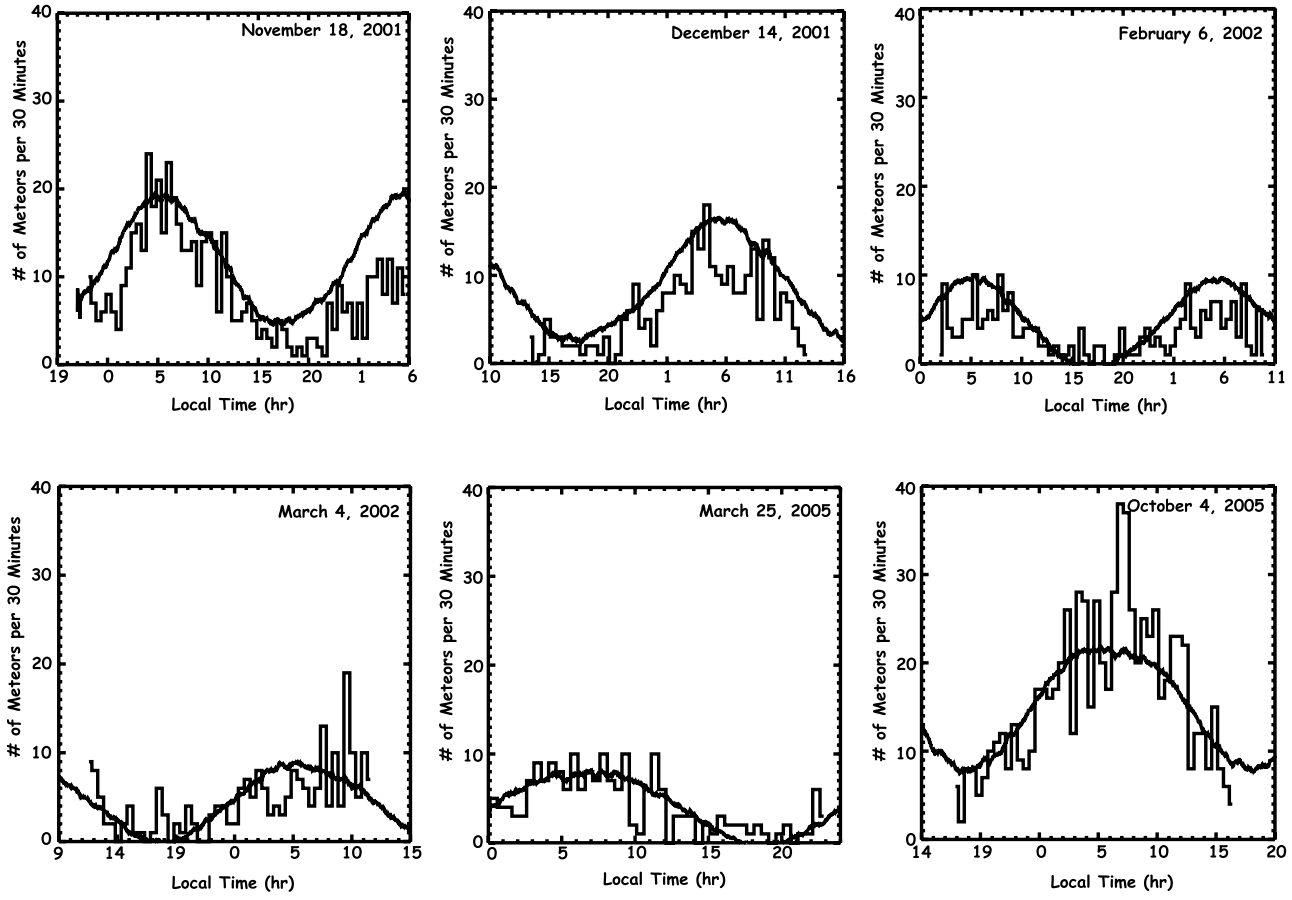

Figure 11. Comparison of the model with observed rates at high northern latitudes using the Sondrestrom radar in Greenland.

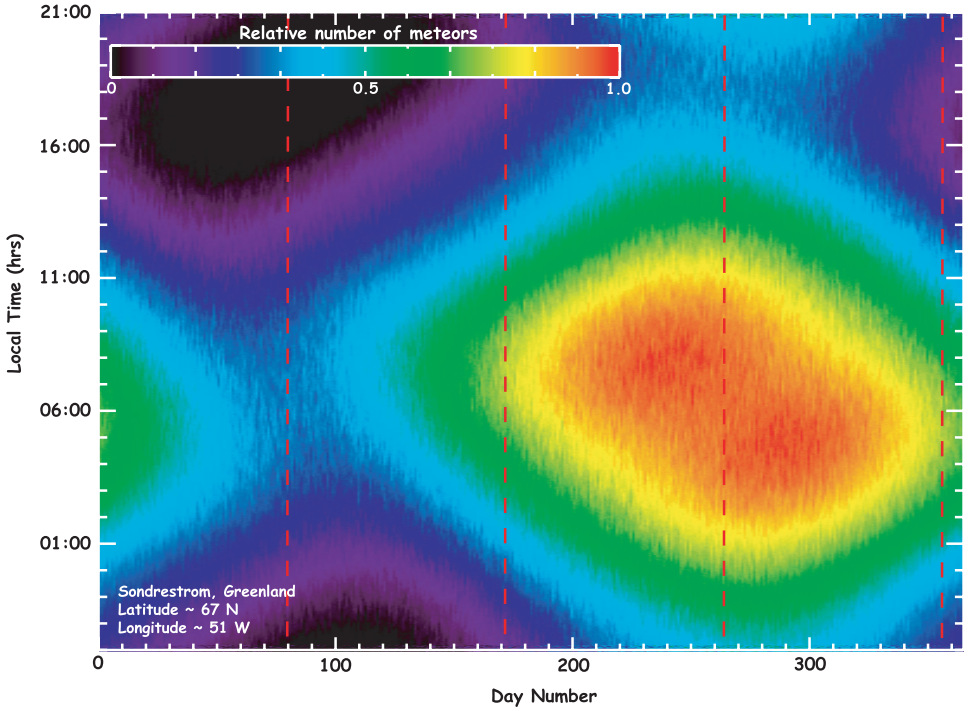

Figure 12. Modeled meteoric influx over a whole year at Sondrestrom-like latitudes.

that during the months when the rate is high there is no diurnal variation on the observed rate, but a variation on the observed azimuth of the meteor distribution. Similar seasonal variability at arctic latitudes is reported by *Singer et al.* [2004]. The scattering mechanisms and geometry of the Antarctic and Arctic measurements, which utilize a conventional meteor radar are very different than those presented here. They detect the radio echo of specular meteor trails from a direction perpendicular to the radar beam. The HPLA observations are based on the detection of the head echo. The meteoroid populations that the HPLA radars and conventional radars detect are also different. We know in fact that HPLA radars are more sensitive and hence they detect smaller particles [*Janches and ReVelle*, 2005]. In addition, since the observed volume is very small they are less sensitive to the larger sizes detected by traditional meteor radars. Nevertheless it is important to outline some of the agreement between the model presented here and those observations.

[27] At the equator the seasonal variation predicted by the model is negligible, while at mid latitudes it is similar to those presented here for the JRO and AO locations (Figures 8 and 9), but is more pronounced as the latitude increases (Figure 13).

[28] In order to understand how well the model predicts the geographical measured variability using the different radars we performed the following exercise. As discussed earlier, to fit the model with the observed rates, we first normalized, for a given observatory, the entire predicted year to that of the seasonal maxima (21 September for AO and Sondrestrom and 21 March for Jicamarca) and then renormalize each curve to the maximum rate at the seasonal peak. If we divide this factor by the assumed radar beam area we can then have an estimate of meteors per minute per kilometer square resulting in ~99 and ~0.3 for AO and Sondrestrom respectively. If we compute the ratio of the maximum rate per minute per kilometer square on 21 September at Sondrestrom latitude to that of Arecibo latitude we obtain a factor of ~0.8 which is ~270 larger than the measured ratio (0.3/99). This implies that Sondrestrom detects much less particles than predicted by the model. This implies that the effects introduced by using higher frequencies is large. We also note that Arecibo will detect smaller particles than Sondrestrom since the latter is less sensitive, thus the discrepancy in the modeled and measured ratio will also be influenced by this effect. We are currently developing a model of the frequency dependance on meteor detectability which will provide a better insight on this issue.

4. Discussion

[29] In the previous section we have presented the results of simulating, using Monte Carlo techniques, the expected micrometeor rate that will occur within a small volume located in the MLT. We have compared the simulations with observations at different seasons and latitudes, finding generally excellent agreement. We have also shown, that in order to simulate the observed rates it is necessary to introduce an empirical effect in the model that effectively sets a limit to the minimum elevation angle that the meteor radiant must have to be detected by the radar. In this section we first discuss the possible instrumental and/or physical effects that could be responsible for setting this threshold.

[30] We argue that the low detectability of low-elevation radiant meteors is probably caused by a combination of physical processes related to the particle interaction with the air molecules upon atmospheric entry. *Love and Brownlee* [1991] published the results of a model, which included 51,000 particles with initial diameters between 10 μm and

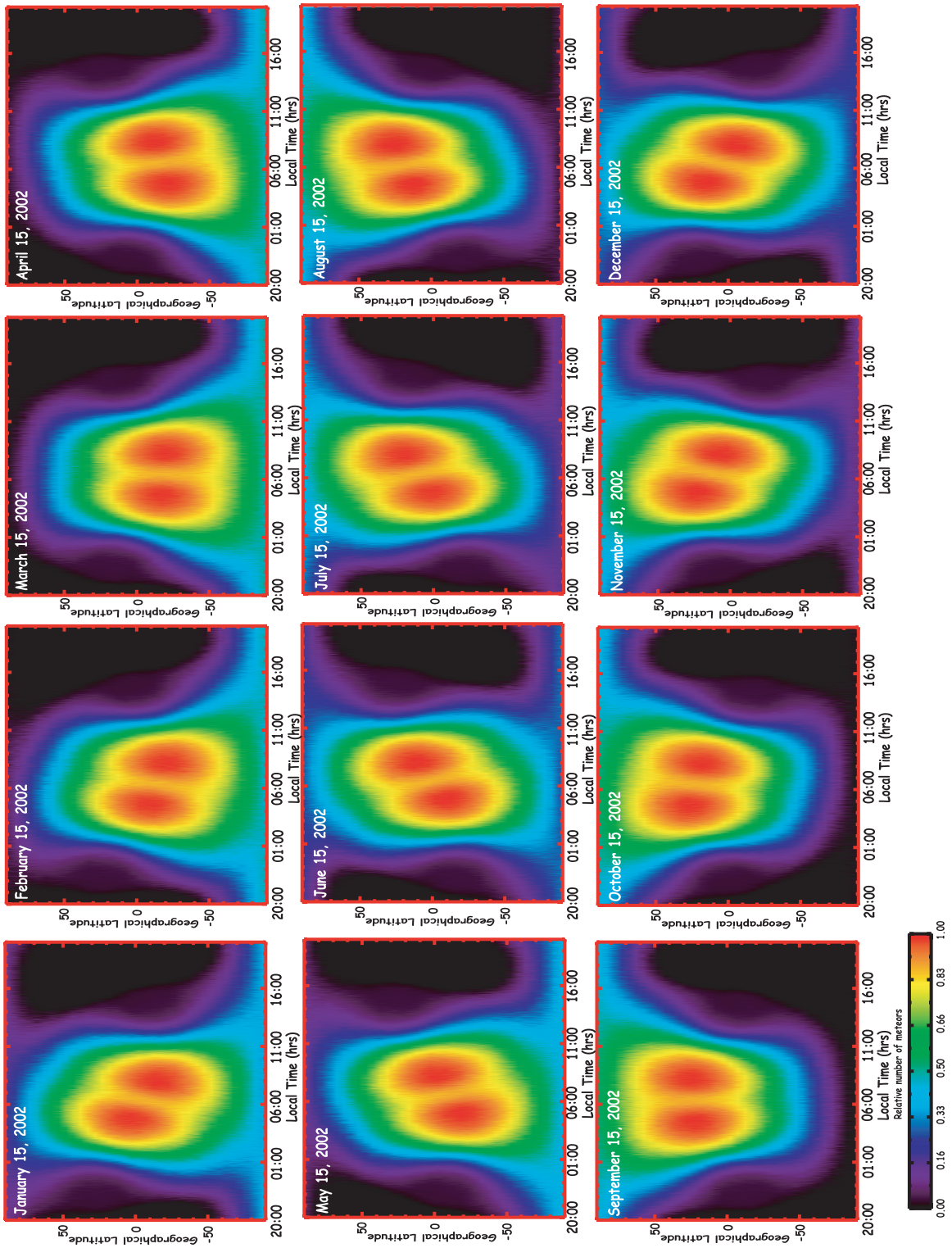

Figure 13. A set of predictions of the global micrometeoric influx for the 15th of each month at a longitude of ~66°W.

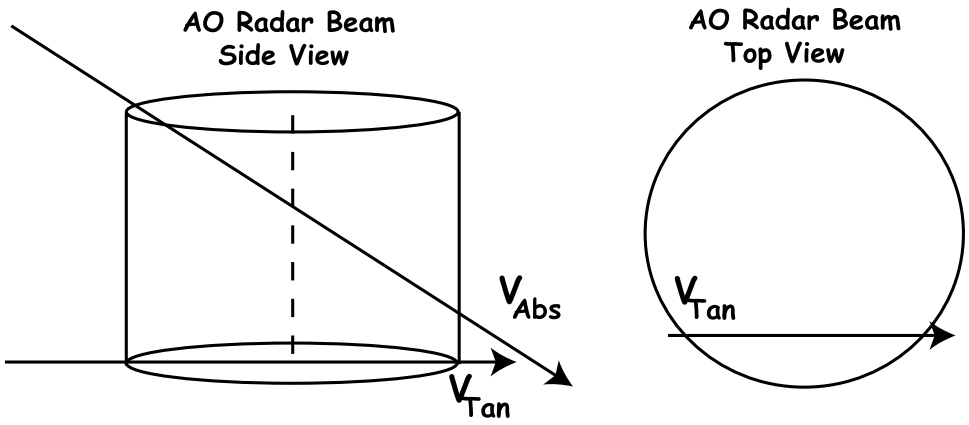

Figure 14. Diagram showing the effect that could be introduced by meteors which have large tangential velocity components while crossing the radar beam.

100 mm. Assuming a melting temperature of ~1350°C the authors concluded that strongest heating occurs between 85 and 100 km of altitudes, independent of size, velocity or entry angle, with half of the sample undergoing strong heating between 85 and 90 km. These altitudes seem to be too low if they are compared with recent micrometeor head echo altitude distributions observed with HPLA radars [*Janches et al.*, 2003; *Janches and ReVelle*, 2005]. This is not surprising since the modeled particles are somewhat larger than those detected by these instruments [*Janches et al.*, 2000b; *Mathews et al.*, 2001; *Close et al.*, 2005]. Nevertheless, the authors showed that shallow atmospheric entry will produce weaker but extended heating processes. If the same effect is produced during the shallow entry of smaller particles, this could prevent the particle from producing enough ionization to exceed the necessary electron density to be observed by the radar but at the same time reach temperatures sufficiently high to deposit part or all the meteoric material at higher altitudes. We also note that for very small elevation angles (<7°) it is possible that most of the particles will skip off the atmosphere and bounce back to the interplanetary space as suggested by the model results presented by *Love and Brownlee* [1991].

[31] The most probable answer for this question is a combination of all these effects. Although in this work a single value of L seems to be enough to simulate the diurnal curves it is entirely possible that the value of this parameter will be a function of the velocity and mass of the entering particle. For example, for a given entry velocity and angle a larger particle will survive and/or produce more electrons than a smaller one and hence have a different elevation threshold. We are currently building models of these processes to be included in this simulation and some preliminary results can be found in the work of *Janches and ReVelle* [2005].

[32] In addition, we argue against two other observational effects for the lack of detectability of low-elevation meteors. These are

[33] 1. **Time of flight**. We first consider the possibility that the disagreement shown in Figure 3 is produced by the inability of detecting low-elevation particles because of their relatively short time of flight through the radar beam. Figure 14 shows a diagram of such effect. A low elevation and fast meteor will have a large tangential velocity component. For example, a particle traveling at 50 km/sec in the tangential direction and through the center of the radar beam will need ~12 msec to cross it. This time includes the meteoroid also traveling through the first side lobes [*Janches et al.*, 2004b]. Since the interpulse period (IPP) used for these observations was 1 msec [*Janches et al.*, 2003], the lifetime of the particle within the radar beam is long enough to obtain several samples of such event. As the meteoroid path moves closer to the edge of the radar beam, the time needed to cross its width will decrease. It is reasonable to think that the probability of detecting a meteor will decrease as the traveling time of the meteor through the radar beam decreases. We performed a simulation of this effect for which we assume a uniform distribution of particle, for a given elevation and velocity, crossing the radar observing volume. Some of the particles will travel closer to the center and hence last longer within the radar beam. Others will travel closer to the edge and last shorter time inside of the volume. In Figure 15 we compare the AO observed rates in January 2002 with the predicted rates. We compare different time thresholds, that is, assuming that a meteor will be detected if the time of flight through the radar beam is greater than a given value. We used four different values and again find disagreement between prediction and observations for all of them. It is clear from these results that this effect will not explain the observed diurnal rate and it is unlikely that is a major factor on filtering low-elevation meteors.

[34] 2. **Aspect sensitivity**. The second scenario is that the head echo is aspect sensitive. That is the radar signal return is stronger for meteors traveling at high-elevation angles (more parallel to the beam axis). However, polarization ratio measurements using the ALTAIR radar system presented by *Close et al.* [2002] showed that the meteor head echo needs to be approximately spherical in shape (i.e., the radar cross section is isotropic) in order to explain their observations. These results suggest that the detection of the head echo will not be strongly aspect sensitive.

[35] Another issue that needs to be discussed in this section is the effect produced in the simulation by changing the size of the modeled volume. As mentioned earlier, the size must be small enough for the flat Earth assumption to apply. However, from the comparison with Arecibo results to that with the JRO and Sondrestrom observations, we

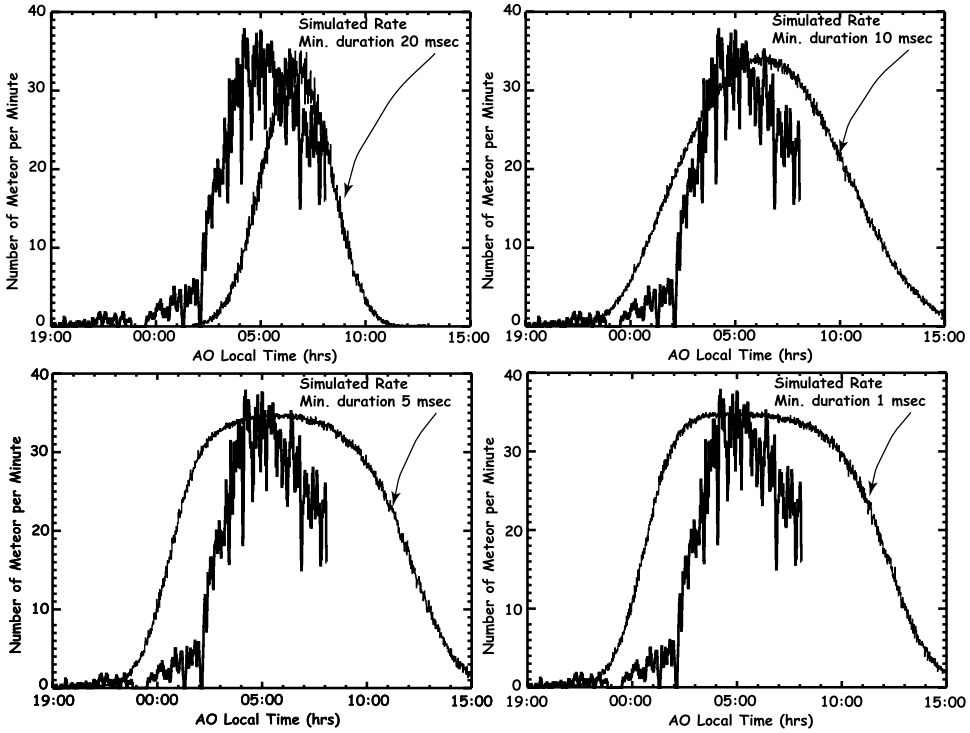

Figure 15. Comparison of the AO observed rates in January 2002 with the predicted rates assuming that a meteor will be detected if the time of flight through the radar beam is greater than a given value.

changed the radius by almost an order of magnitude from 0.3 to 1 km. As expected, the differences in the beam size it is not manifested on the diurnal and/or seasonal trend of the occurrence rate, but in the increase of the number of particles and upper limit of the meteoroid size (or mass) detected. For example, the highest particle radius detected on the AO beam for one day simulation using the mass function described earlier is $\sim$3 μm, while for Sondrestrom and JRO was $\sim$30 μm. This is assuming a meteoroid mass density of 3 g per cc. The lowest size limit is not affected by changing the detecting volume. This limit will be, most likely, set by the radar sensitivity which is not yet included in the model, but it is expected that AO will detect smaller particles than JRO or Sondrestrom because of its higher sensitivity.

5. Summary

[36] In this work we have presented a simple model using Monte Carlo simulation techniques that predicts fairly accurately the observed diurnal and seasonal trend of the micrometeor influx rate detected by HPLA radars at two different sites. The simulation assumes that the radar observing volume is a cylinder and that the particles will be first observed at an altitude calculated from the meteor energy equation approximated for small particles [*Janches and ReVelle*, 2005]. The model also assumes that the incoming flux originates uniformly over the year and the main source of particles originates from an apex-centered particle population as observed recently by JRO [*Chau and Woodman*, 2004; *Sulzer*, 2004; *Janches and Chau*, 2005]. The small-scale details of the observed Arecibo diurnal rates are reproduce by the contribution of two secondary meteor populations known as helion and antihelion which, according to the results presented here, provide only $\sim$30% of the total number of particles while the apex-centered distribution provides the remain $\sim$70%. Recently, *Galligan and Baggaley* [2005] reported meteor radiant measurements from a large data set obtained with the AMOR system in New Zealand. The authors claimed to have measured a noticeable difference between the number of particles with radiant belonging to the antihelion (AH) population to that originating from the helion (H). This difference results in $\sim$1.3 more particles from the AH than the H source after the radiants were corrected by a number of effects. For our model, we have assumed that both sources provide equal amount of particles at a given time (1/6 each). This assumption results in excellent agreement thus far with the observations presented in this work. We also show that for a given location, the contribution of each meteor population varies as a function of season. To obtain agreement between model and observations we have included an empirical model of an atmospheric effect that effectively sets a limit to the minimum elevation that the meteoroid radiant must have to be detected by the radar. We discussed different processes that could be responsible for this effect. We used the model to predict the observations at higher latitudes and to predict also the global and annual influx of these particle populations. Future work will include ablation and electron production models to attempt to explain physically the need for the threshold on the elevation angle.

[37] **Acknowledgments.** The Arecibo Observatory is part of the National Astronomy and Ionosphere Center, which is operated by Cornell University under cooperative agreement with the National Science Foundation. The Jicamarca Radio Observatory is a facility of the Instituto Geofísico del Perú and is operated with support from the NSF Cooperative

Agreement ATM-0432565 through Cornell University. The Sondrestrom Facility is operated for NSF by SRI International under cooperative agreement ATM-0334122. D.J. and A.C. have been supported under NSF grants ATM-0422043 to the University of Colorado at Boulder and ATM-05311464 to NorthWest Research Associates, Inc.

[38] Wolfgang Baumjohann thanks Lars Dyrud and Philip J. Erickson for their assistance in evaluating this paper.

References

Baggaley, W. J. (2002), Radar observations, in *Meteors in the Earth's Atmosphere*, edited by E. Murad and I. P. Williams, pp. 123–148, Cambridge Univ. Press, New York.

Breakall, J. K., and J. D. Mathews (1982), A theoretical and experimental investigation of antenna near-field effects as applied to incoherent backscatter measurements at Arecibo, *J. Atmos. Terr. Phys.*, *44*(5), 449–454.

Brown, P. G., R. E. Spalding, D. O. ReVelle, E. Tagliaferri, and S. P. Worden (2002), The flux of small near-Earth objects colliding with the Earth, *Nature*, *420*, 294–296.

Ceplecha, Z., J. Borovička, W. G. Elford, D. O. ReVelle, R. L. Hawkes, V. Porubčan, and M. Šimek (1998), Meteor phenomena and bodies, *Space Sci. Rev.*, *84*, 327–471.

Chau, J. L., and R. F. Woodman (2004), Observations of meteor head-echoes using the Jicamarca 50 MHz radar in interferometer mode, *Atmos. Chem. Phys.*, *4*, 511–521.

Close, S., S. M. Hunt, M. J. Minardi, and F. M. McKeen (2000), Analysis of Perseid meteor head echo data collected using the Advance Research Project Agency Long-Range Tracking and Instrumentation Radar (ALTAIR), *Radio Sci.*, *35*, 1233–1240.

Close, S., M. Oppenheim, S. M. Hunt, and L. Dyrud (2002), Scattering characteristics of high-resolution meteor head echoes detected at multiple frequencies, *J. Geophys. Res.*, *107*(A10), 1295, doi:10.1029/2002JA009253.

Close, S., M. Oppenheim, D. Durand, and L. Dyrud (2005), A new method for determining meteoroid mass from head echo data, *J. Geophys. Res.*, *110*, A09308, doi:10.1029/2004JA010950.

Cziczo, D. J., D. S. Thomson, and D. M. Murphy (2001), Ablation, flux, and atmospheric implications of meteor inferred from stratospheric aerosol, *Science*, *291*, 1772–1775.

Dyrud, L. P., K. Denney, J. Urbina, D. Janches, E. Kudeki, and S. Franke (2005), The meteor flux: It depends how you look, *Earth Moon Planets*, *95*, 89–100.

Erickson, P. J., F. D. Lind, S. M. Wendelken, and M. A. Faubert (2001), Meteor head echo observations using the Millstone-Hill, UHF incoherent scatter radar system, in *Proceedings of the Meteoroids 2001 Conference, 6–10 August 2001, Kiruna, Sweden*, edited by B. Warmbein, ESA SP-495, pp. 457–463, Eur. Space Res. Technol. Cent., Noordwijk, Netherlands.

Galligan, D. P., and W. J. Baggaley (2005), The radiant distribution of AMOR radar meteors, *Mon. Not. R. Astron. Soc.*, *359*(2), 551–560.

Hughes, D. W. (1978), Meteors, in *Cosmic Dust*, edited by J. A. M. McDonnell, pp. 123–186, Wiley-Interscience, Hoboken, N. J.

Hunt, S. M., M. Oppenheim, S. Close, P. G. Brown, F. McKeen, and M. Minardi (2004), Determination of the meteoroid velocity distribution at the Earth using high-gain radar, *Icarus*, *168*, 34–42.

Janches, D., and J. L. Chau (2005), Observed diurnal and seasonal behavior of the micrometeor flux using the Arecibo and Jicamarca radars, *J. Atmos. Sol. Terr. Phys.*, *67*, 1196–1210.

Janches, D., and D. O. ReVelle (2005), The initial altitude of the micrometeor phenomenon: Comparison between Arecibo radar observations and theory, *J. Geophys. Res.*, *110*, A08307, doi:10.1029/2005JA011022.

Janches, D., J. D. Mathews, D. D. Meisel, V. S. Getman, and Q. H. Zhou (2000a), Doppler studies of near-antapex UHF radar micrometeors, *Icarus*, *143*, 347–353.

Janches, D., J. D. Mathews, D. D. Meisel, and Q. H. Zhou (2000b), Micrometeor observations using the Arecibo 430 MHz radar: I. Determination of the ballistic parameter from measured Doppler velocity and deceleration results, *Icarus*, *145*, 53–63.

Janches, D., D. D. Meisel, and J. D. Mathews (2001), Orbital properties of the Arecibo micrometeors at Earth interception, *Icarus*, *150*, 206–218.

Janches, D., A. Pellinen-Wannberg, G. Wannberg, A. Westman, I. Haggstrom, and D. D. Meisel (2002), Tristatic observations of meteors using the 930 MHZ EISCAT radar system, *J. Geophys. Res.*, *107*(A11), 1389, doi:10.1029/2001JA009205.

Janches, D., M. C. Nolan, D. D. Meisel, J. D. Mathews, Q. H. Zhou, and D. E. Moser (2003), On the geocentric micrometeor velocity distribution, *J. Geophys. Res.*, *108*(A6), 1222, doi:10.1029/2002JA009789.

Janches, D., S. E. Palo, E. M. Lau, S. K. Avery, J. P. Avery, S. de la Peña, and N. A. Makarov (2004a), Diurnal and seasonal variability of the meteoric flux at the South Pole measured with radars, *Geophys. Res. Lett.*, *31*, L20807, doi:10.1029/2004GL021104.

Janches, D., M. C. Nolan, and M. P. Sulzer (2004b), Radiant measurement accuracy of micrometeors detected by the Arecibo 430 MHz dual-beam radar, *Atmos. Chem. Phys.*, *4*, 621–626.

Jones, J., and P. G. Brown (1993), Sporadic meteor radiant distribution: Orbital survey results, *Mon. Not. R. Astron. Soc.*, *265*, 524–532.

Love, S. G., and D. E. Brownlee (1991), Heating and thermal transformation of micrometeoroids entering the Earth's atmosphere, *Icarus*, *89*, 26–43.

Love, S. G., and D. E. Brownlee (1993), A direct measurement of the terrestrial mass accretion rate of cosmic dust, *Science*, *262*, 550–553.

Mathews, J. D., D. Janches, D. D. Meisel, and Q. H. Zhou (2001), The micrometeoroid mass flux into the upper atmosphere: Arecibo results and a comparison with prior estimates, *Geophys. Res. Lett.*, *28*, 1929–1932.

Pellinen-Wannberg, A., A. Westman, G. Wannberg, and K. Kaila (1998), Meteor fluxes and visual magnitudes from ESICAT radar event rates: A comparison with cross-section based magnitude estimates and optical data, *Ann. Geophys.*, *116*, 1475–1485.

Plane, J. M. C. (2004), A new time-resolved model for the mesospheric Na layer: Constraints on the meteor input function, *Atmos. Chem. Phys.*, *4*, 627–638.

ReVelle, D. O. (2001), Global infrasonic monitoring of large bolides, in *Proceedings of the Meteoroids 2001 Conference, 6–10 August 2001, Kiruna, Sweden*, edited by B. Warmbein, ESA SP-495, pp. 483–490, Eur. Space Res. Technol. Cent., Noordwijk, Netherlands.

ReVelle, D. O. (2005), The mesopause as a physical penetration boundary, *J. Atmos. Sol. Terr. Phys.*, *67*, 1159–1170.

Sato, T., T. Nakamura, and K. Nishimura (2000), Orbit determination of meteors using the MU radar, *IEICE Trans. Commun.*, *E83-B*(9), 1990–1995.

Singer, W., J. Weiß, and U. von Zahn (2004), Diurnal and annual variation of meteor rates at the Arctic Circle, *Atmos. Chem. Phys.*, *4*, 1355–1363.

Sulzer, M. P. (2004), Meteoroid velocity distribution derived from head echo data collected at Arecibo during regular world day observations, *Atmos. Chem Phys.*, *4*, 947–954.

Taylor, A. D. (1995), The Harvard radio meteor project meteor velocity distribution reappraised, *Icarus*, *116*, 154–158.

Taylor, A. D. (1997), Radiant distribution of meteoroids encountering the Earth, *Adv. Space Res.*, *20*(8), 1505–1508.

Taylor, A. D., and W. G. Elford (1998), Meteoroid orbital element distribution at 1 AU deduced from the Harvard radio meteor project observations, *Earth Planets Space*, *50*, 569–575.

von Zahn, U., J. Höffner, and W. J. McNeil (2002), Meteor trails as observed by lidars, in *Meteors in the Earth's Atmosphere*, edited by E. Murad and I. P. Williams, Cambridge Univ. Press, New York.

Wasson, J. T., and F. T. Kyte (1987), Comment on the letter "On the influx of small comets into the Earth's atmosphere. II: Interpretation,", *Geophys. Res. Lett.*, *14*, 779–780.

Williams, I. P., and E. Murad (2002), *Meteors in the Earth's Atmosphere*, edited by E. Murad and I. P. Williams, Cambridge Univ. Press, New York.

Yrjölä, I., and P. Jenniskens (1998), Meteor stream activity. VI: A survey of annual meteor activity by means of forward meteor scattering, *Astron. Astrophys.*, *330*, 739–752.

A. Chandran, Department of Aerospace Engineering Sciences, University of Colorado, 429 UCB, Boulder, CO 80309-0429, USA. (amal.chandran@colorado.edu)

J. L. Chau and R. Woodman, Radio Observatorio de Jicamarca, Instituto Geofísico del Perú, Apdo. 130207, Lima 13, Perú. (jchau@jro.igp.gob.pe)

C. J. Heinselman, SRI International, 333 Ravenswood Avenue, Menlo Park, CA 94025, USA. (craig.heinselman@sri.com)

D. Janches, NorthWest Research Associates Inc., CoRA Division, 3380 Mitchell Lane, Boulder, CO 80301, USA. (diego@cora.nwra.com)